ACCEPTED MANUSCRIPT

Title: Application of frame motion and mesh motion techniques for determining the torque of a Rushton turbine.

Authors: Michał Duda, Wojciech Sobieski

To appear in: Technical Sciences

Received 22 December 2025;

Accepted 4 February 2026;

Available online 19 March 2026.

Correspondence: Michał Duda, Katedra Elektrotechniki i Energetyki, Wydział Nauk Technicznych, Uniwersytet Warmińsko-Mazurski, ul. Oczapowskiego 11, 10-719 Olsztyn, e-mail: michal.duda@uwm.edu.pl

DOI: https://doi.org/10.31648/

APPLICATION OF FRAME MOTION AND MESH MOTION TECHNIQUES FOR DETERMINING THE TORQUE OF A RUSHTON TURBINE

Michał Duda ORCID: 0000-0002-9174-3840***, Wojciech Sobieski*** ORCID: 0000-0003-1434-5520

University of Warmia and Mazury, Olsztyn, Poland

Received ……., accepted ……, available online ……. .

Key words: Rushton turbine, CFD, Multiple Reference Frame, Sliding Mesh, Volume of Fluid.

Abstract

The article presents experimental and numerical studies of the torque of a Rushton turbine impeller operating in a cylindrical tank without partitions. The analyses were carried out on a laboratory scale for one system geometry and five impeller rotational speeds. Numerical calculations were performed using the Multiple Reference Frame (MRF) and Sliding Mesh (SM) methods in combination with the Volume of Fluid (VoF) model, with an analysis of the influence of mesh density performed prior to the main calculations. The simulations were performed in the ANSYS Fluent environment, while the experimental measurements were performed using the IKA EUROSTAR 60 control drive. The results obtained showed good qualitative agreement of the torque characteristics as a function of rotational speed, with simultaneous quantitative discrepancies consisting in obtaining higher torque values in numerical simulations compared to the experiment. These discrepancies may result from the limitations of the RANS approach in mapping global vortex motion and free surface deformation of the liquid, as well as from measurement uncertainties, which indicates further directions for research.

Introduction

Mechanical mixers are widely used in many industries, including the food, chemical, cosmetics, and pharmaceutical industries, as well as in wastewater treatment and biomass processing. Among the various mixer designs, the Rushton turbine is one of the most widely used impeller types – a solution characterized by a simple, compact design and excellent mixing properties. Thanks to these features, it is widely used in processes requiring intensive homogenization, emulsification, and dissolution of substances, as well as in maintaining the homogeneity of liquid and semi-liquid mixtures. This impeller is also used wherever efficient mass and heat exchange and effective aeration of liquids are crucial.

In the context of the real needs of industry and the dynamic development of digital design techniques for process equipment, it is particularly important to support the engineering process through simulation methods. One of the key aspects of mixer design – often already at the quotation stage – is the accurate estimation of the drive unit parameters, in particular the power requirement. Underestimating this value can lead to installation malfunctions, increased failure rates, and production losses. Overestimating, on the other hand, results in excessive investment and operating costs.

In engineering practice, at least in Poland, the methods described in Streka's classic monograph (STREK 1971) are still often used to estimate mixing power. Although historically significant, this monograph does not take into account many contemporary mixer designs or modern operating conditions. Meanwhile, design is now almost always carried out in a three-dimensional environment, which means that the geometries of tanks and mixers are available in digital form. At the same time, the development of computational fluid dynamics (CFD) methods and the wide availability of both software and knowledge in this field open up new possibilities for more accurate and flexible determination of mixer operating parameters. In this context, replacing outdated analytical methods with numerical simulations seems not only justified, but even necessary. Based on simulations, it is possible to obtain the value of the torque acting on the impeller during its operation – this issue is the main topic of this article.

Previous studies demonstrate that cylindrical stirred tanks equipped with Rushton turbine impellers, both with and without baffles, constitute a well-established subject of numerical and experimental research. Research includes, for example: experimental and numerical analysis of the velocity field (KYSELA et al. 2014, KOYRO et al. 2022, ALAM et al. 2022), the influence of the position of the rotating zone interface (PATIL et al. 2018), the influence of the number of blades (TILL et al. 2019), and the influence of the diameter of the blades and their angle of inclination on the operation of the stirred tank (PHUMNOK et al. 2024). It can be noted that studies usually focus on specific aspects

for selected operating conditions, and it is difficult to find specific characteristics presenting the impeller torqueas a function of rotational speed. Despite the breadth of existing studies, the majority of published works concentrate primarily on flow field characterization, turbulence structures, or mixing efficiency indicators. While several experimental and numerical investigations explicitly account for free-surface deformation and central vortex formation in unbaffled tanks (e.g. TALAGA, DUDA 2020, PŁUSA et al. 2021), these effects are most often analyzed in terms of flow topology and mixing dynamics rather than their direct influence on impeller torque and power characteristics. Quantitative determination of the impeller torque as a function of rotational speed, particularly supported by direct experimental measurements and CFD simulations using both MRF and SM approaches, remains relatively underrepresented in the available literature. The present study addresses this gap by combining experimental torque measurements with numerical simulations, including VoF-based modeling of the free surface.

Materials and methods

Determining mixing power using the experimental method

The laboratory tests used an IKA EUROSTAR 60 control drive with a speed range of 30 to 2000 rpm and a maximum torque of 0.6 N·m. According to the manufacturer's data, the speed setting accuracy is ±1 rpm, while the speed measurement deviation is ±1% for values above 300 rpm and ±3 rpm for lower speeds. According to the product data sheet, the declared torque measurement accuracy is ±0.06 N·m. To reduce the influence of drive and bearing losses, a differential measurement approach was applied. For each rotational speed, three repeated measurements were performed and the torque was calculated as

$$M = M_{\text{wet}} - M_{\text{dry}} \tag{1}$$

where: M_{wet} – denotes the torque measured with liquid in the tank [N·m], and M_{dry} – denotes the torque measured under identical operating conditions without liquid, representing mechanical losses of the drive system [N·m].

The values obtained in the experiment correspond to the mean of three differential measurements. The error bars represent 95% confidence intervals of the mean, determined based on the t-Student distribution (df = 2), and reflect the uncertainty of the mean value estimation.

The tests were performed using a six-bladed Rushton impeller with an outer diameter of 0.065 m. A diagram of the experimental setup is shown in Figure 1.

a)

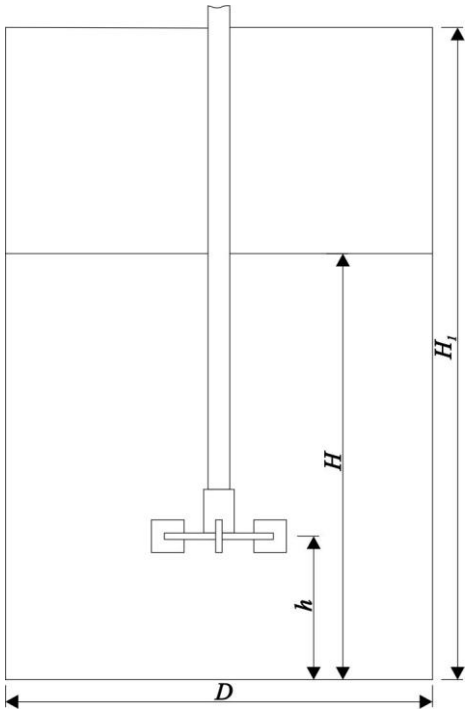

c)

No.	Name	Expression [m]
1	D	0.195
2	H_1	0.300
3	H	0.195
4	h	0.065
5	a	0.018
6	b	0.015
7	c	0.003
8	d	0.065
9	d_1	0.010
10	d_2	0.014

b)

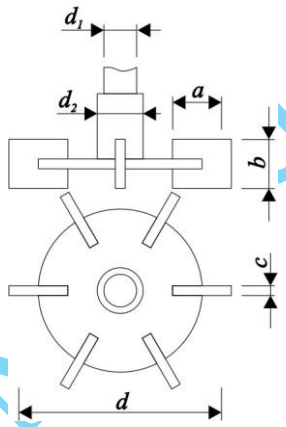

d)

Fig. 1. Laboratory workstation: a) geometry of the tank with the impeller, where H denotes the liquid filling height and H = D (internal tank diameter), and h = H/3; b) impeller geometry; c) tank and impeller geometric parameters; d) photograph of the laboratory workstation

The working medium was water at a temperature of 20±0.5 °C. The water was placed in a glass cylindrical tank with an internal diameter D = 0.195 m and a height of H_1=0.300 m. The impeller was installed in such a way that the horizontal axis of the impeller was located 0.65 m above the bottom of the tank, which corresponded to 1/3 of the liquid filling height (h = H/3).

Determining mixing power using simulation methods

The simulation studies used the Finite Volume Method, based on standard equations (*Ansys Fluent Theory Guide* 2022, SOBIESKI 2025) of mass balance:

$$\frac{\partial \rho}{\partial t} + div(\rho \vec{v}) = 0 \tag{2}$$

and momentum balance:

$$\frac{\partial (\rho \vec{v})}{\partial t} + div\left(\rho \vec{v}\vec{v} + p\overleftrightarrow{I}\right) = div(\overleftrightarrow{\tau}^{l} + \overleftrightarrow{\tau}^{t}) + \rho s_b, \tag{3}$$

where: ρ – density [kg/m^3], $\vec{v}$ – velocity [m/s], p – static pressure [Pa], $\overleftrightarrow{\tau}^l$ – viscous stress tensor [Pa], $\overleftrightarrow{\tau}^t$ – turbulent stress tensor [Pa], s_b – source of forces [N/m^3].

The system of equations (2–3) describes the behavior of a single medium in a stationary reference frame. In the case of mixing systems consisting of a tank and an impeller, there is relative movement of the elements, which must be taken into account in the model. One of three techniques is used for this purpose: Single Reference Frame (SRF), Multiple Reference Frame (MRF), or Sliding Mesh (SM). In the SRF and MRF approaches, the system of equations (2–3) is modified to take into account the rotational motion of selected parts of the computational domain (e.g., the area covering the impeller) relative to the stationary part (e.g., the tank). Details of the modified mathematical model can be found, among others, in the documentation of the software used and are not discussed here (*Ansys Fluent Theory Guide* 2022). Similarly, other general issues, such as the description of popular turbulence models, have been omitted.

SRF involves solving motion equations in a single rotating reference frame covering the entire computational domain. This technique is most commonly used for stationary analyses in situations where the average effect of impeller motion on the flow is important, without considering direct interaction with stationary elements. MRF involves dividing the domain into several zones, each of which can be defined in a different reference frame (e.g., the impeller zone in a rotating frame, the tank in a stationary frame). Transitions between zones are modeled assuming a steady state. MRF is a quasi-stationary method that allows local motion to be mapped without the need for a full time simulation. The SFR and MRF approaches are sometimes referred to as "frozen rotor" techniques, as the simulation always concerns a single, selected position of the rotor relative to the tank walls (although in the case of a tank without partitions the angular position of the impeller relative to the tank walls is geometrically irrelevant, while the global flow behavior remains strongly influenced by circular circulation and free-surface deformation). SM is a method in which the computational grid actually moves over time. It enables the simulation of unsteady flows with accurate representation of the time-varying position of rotating elements. SM is the most computationally expensive, but offers the highest accuracy in analyzing flow dynamics and the interaction of moving parts with their environment. In the case of SRF, the entire numerical grid is subject to virtual rotation (Fig. 2). In the case of MRF or SM, there are at least two grid zones, and data between them is transferred via a so-called interface (Fig. 3). This interface can be compatible (as in MRF), which means that cells on both sides of the interface share nodes located on the interface, or incompatible (as in SM), which means that the nodes are duplicated so that both meshes can move relative to each other without deforming the cells contacting the interface.

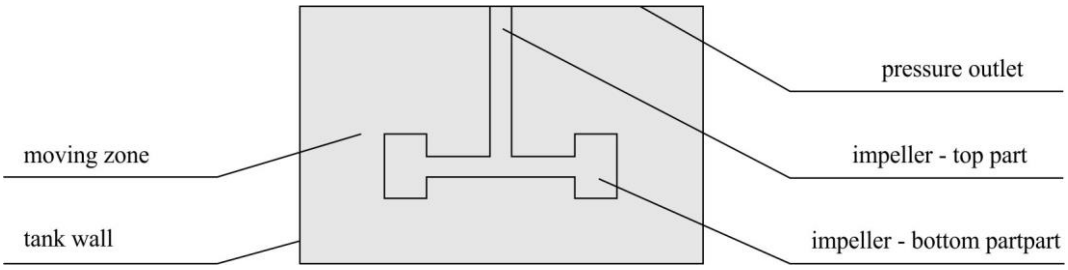

Fig. 2. Diagram of an impeller with one mesh zone

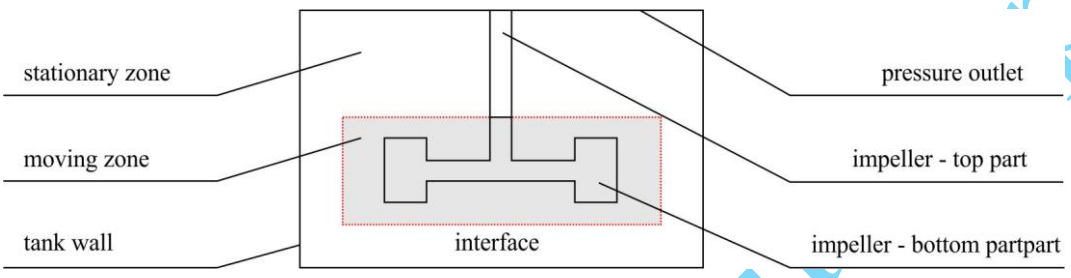

Fig. 3. Diagram of an impeller with two mesh zones separated by an interface (compatible or incompatible)

In Figures 2 and 3, the moving zone is marked in gray. If the upper surface of the moving zone does not coincide with the upper surface of the tank (as is the case in Fig. 3), the impeller shaft will be divided into two parts as a result of dividing the computational domain into zones. It is important to remember to assign the appropriate angular velocity (the same as in the moving zone) to the part outside the moving zone, which can be achieved by applying appropriate boundary conditions.

Results and discussion

Experimental research

The experimental tests were carried out on the test bench described in Determining mixing power using the experimental method. In order to measure the torque, three stages of impeller operation were distinguished: acceleration to a set speed for 30 seconds, operation at a constant speed for 120 seconds, and deceleration to a standstill for 30 seconds. Before each series of measurements, the impeller was operated for 15 minutes to warm up the oil bearings in the drive. The torque value was recorded from the control panel at the end of the second stage, i.e., during the steady-state operation of the impeller. Measurements were taken for five impeller speeds: 480, 420, 360, 300, and 240 rpm. Each measurement was repeated three times and the results were averaged. In all cases, the tank was filled with water to a height of H = 0.195 m,

corresponding to approximately 2/3 of the total tank height (H_1 = 0.300 m), as shown in Figure 1a. The quantitative results of the torque measurements are presented later in this paper. The measured torque ranged from 0.015 to 0.005 N·m for the highest and lowest rotational speeds, respectively.

Impeller geometry

The geometry of the impeller was prepared in the ANSYS SpaceClaim module based on the experimental setup shown in Figure 1. All dimensions and geometric features correspond exactly to those used in the laboratory experiments. The mixing tank was cylindrical, with an internal diameter D = 0.195 m and a total height of H_1 = 0.300 m. A standard Rushton turbine was used as the impeller. It consisted of a disk with a diameter of 0.050 m and a thickness of 0.003 m, equipped with six rectangular blades (0.018 × 0.015 × 0.003 m). The blades were arranged so that the outer diameter of the impeller was d = 0.065 m. The disk was mounted on a shaft with a diameter of d_1 = 0.010 m. A stiffening ring (outer diameter d_2 = 0.014 m, height 0.017 m) was located at the shaft end, directly above the disk. The impeller was mounted coaxially with the tank axis, and the horizontal axis of the impeller was located h = 0.065 m above the bottom of the tank. In the present study, the impeller position is defined by the vertical location of the impeller disk axis relative to the tank bottom, which is a commonly used and unambiguous reference for both experimental and numerical configurations. A detailed schematic with all dimensions is provided in Figure 1a–c.

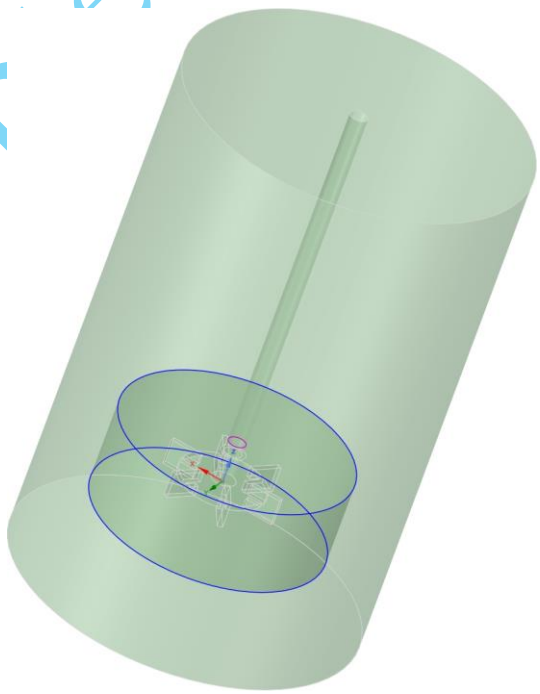

Fig. 4. View of the computational domain divided into a moving and stationary zone

The computational domain (Fig. 4) was divided into two zones: mobile and stationary, in accordance with the requirements of MRF and SM techniques. The mobile part had the shape of a cylinder with a diameter of 0.132 mm and a height of 0.050 m. The diameter of this zone was selected so that the interface between the zones (marked with blue lines in the figure) was located halfway between the outer edges of the stirrer and the tank wall. The height of the zone was set so that the stiffening ring was completely inside the moving area. In the case of the MRF technique, both zones had to be joined with the "Share" tool, which resulted in a compatible interface.

Mesh test

The first stage of modeling was to prepare three mesh variants (mesh 1, mesh 2 and mesh 3) for a stationary model using the MRF technique. The meshes were generated in the ANSYS Mesh module and then converted in the ANSYS Fluent environment into polyhedral meshes, which have fewer cells while maintaining comparable geometry representation quality. After converting the mesh, it was necessary to divide the mesh again into partitions assigned to individual processes (parallel simulations were performed on 4 processes in the study). This approach was recommended by representatives of ANSYS.

Each mesh consisted of two regions corresponding to the moving and stationary zones, in accordance with the previously developed model geometry. The mesh variants differed only in the value of the global or local "Element Size" parameter, which was used to control the mesh density. In mesh 2, only the interior of the domain was densified, while in mesh 3, both the interior of the domain and the mesh adjacent to the impeller surface were densified. In addition, layers of wall mesh were applied to all walls of the impeller and the tank. However, additional mesh refinement in the interface area between the moving and stationary zones was not applied because, as subsequent calculations showed, the scalar fields were continuous there and the transitions between the zones were smooth. The parameters of the numerical meshes are listed in Table 1, and their visualization is shown in Figures 5 and 6. The last column of the table shows the relative calculation time, with mesh 1 as the reference value (on the computer used, it was 3415 s). The mesh test was performed only for the highest rotational speed, for which the dynamic and viscous effects are greatest.

Table 1

Parameters of numerical grids

	Mesh 1	Mesh 2	Mesh 3
Mesh: Element Size (global)	0.005	0.0025	0.0025
Mesh: Element Size (local)	0.001	0.001	0.0025
Mesh: Number of cells (tetrahedral)	1012143	2344245	4081736
Mesh: Max. Skewness	0.80404	0.80141	0.83591
Mesh: Min. Orthogonal Quality	0.19596	0.19859	0.16409
Fluent: Number of cells (polyhedra)	349978	704185	1247360
Relative calculation time	1	2.02	3.47

Source: own elaboration based on data from ANSYS Fluent.

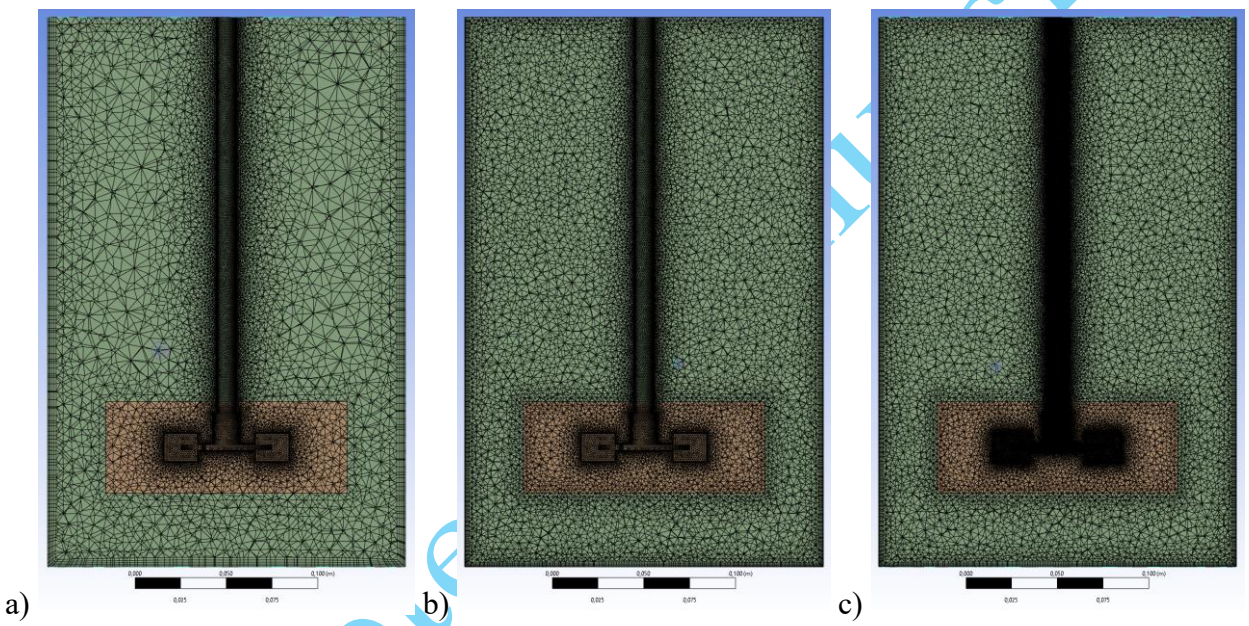

Fig. 5. Quadrangular numerical meshes: a) mesh 1, b) mesh 2, c) mesh 3

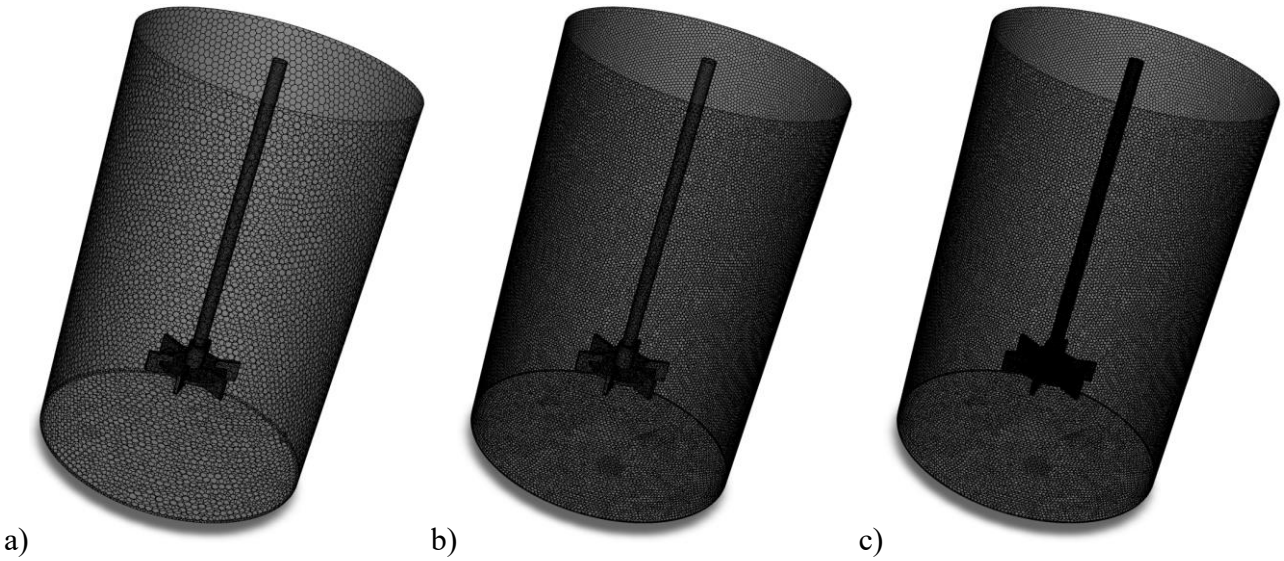

Fig. 6. Polyhedral numerical meshes: a) mesh 1, b) mesh 2, c) mesh 3

In order to monitor changes in characteristic system parameters during the simulation, the value of the torque acting on the impeller (Fig. 7), the mass of water in the tank (Fig. 8), and the average velocity in the computational domain (Fig. 9) were tracked. The mass was monitored in particular to detect any problems with the transfer of values between grid zones in the interface area. The results of calculations for 1000 iterations showed that even mesh 1 provided sufficient accuracy. Further densification of the mesh within the computational domain in mesh 2 and mesh 3 did not significantly affect the results obtained. Similarly, increasing the mesh density in the impeller area in mesh 3 – although it could potentially affect the torque value (calculated based on data from mesh cells adjacent to the impeller walls, of which there were more in mesh 3) – did not result in any noticeable changes. Therefore, mesh 1 was selected for further analysis.

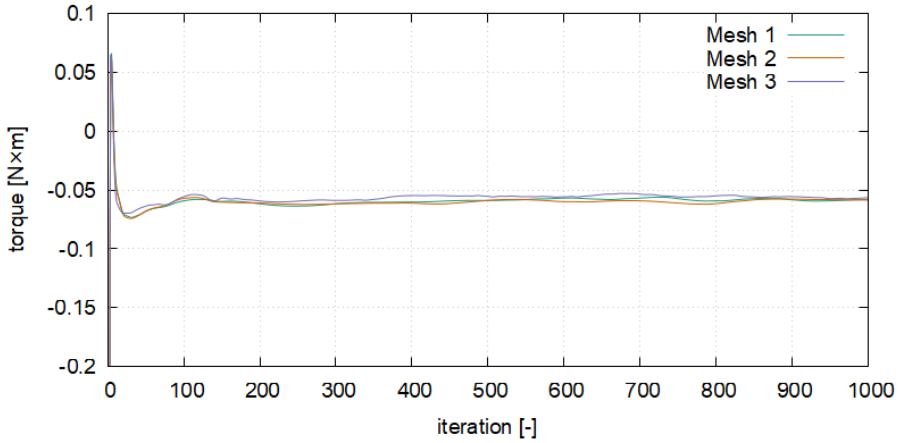

Fig. 7. Torque monitor graph for the MRF model, 480 rpm, and three grid variants

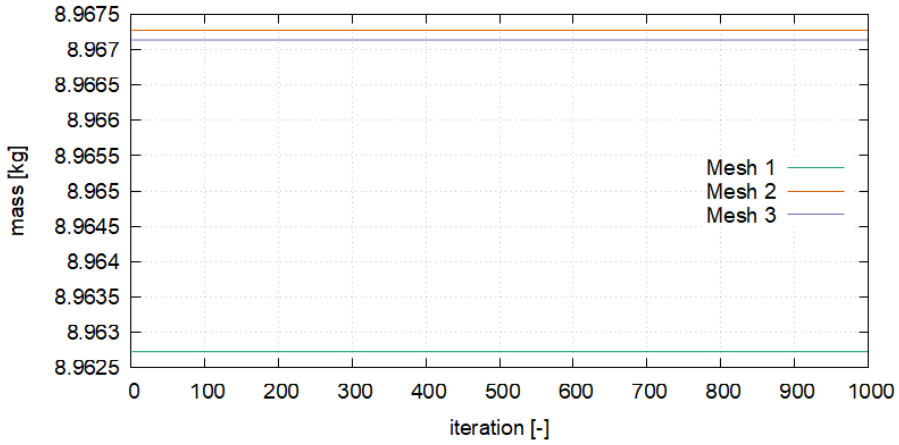

Fig. 8. Mass monitor graph for the MRF model, 480 rpm, and three mesh variants

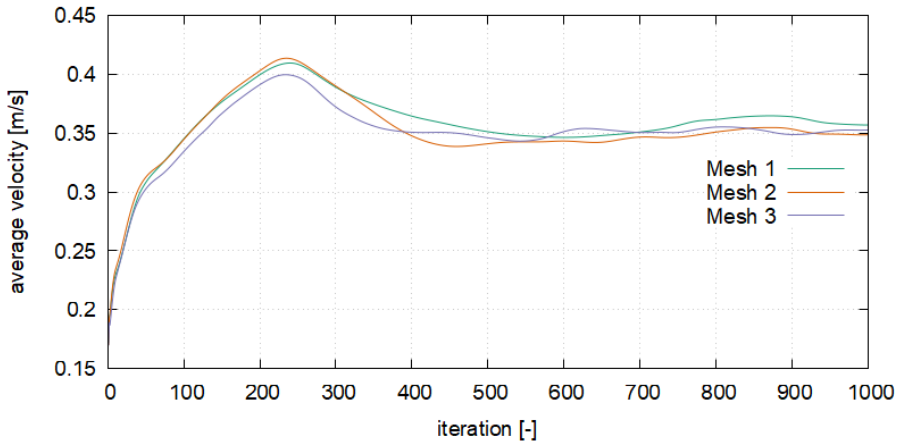

Fig. 9. Average speed monitor graph for the MRF model, 480 rpm, and three mesh variants

Numerical simulations MRF

In the first phase of numerical modeling, a stationary approach was adopted, in which rotational motion was assigned to both the moving zone (using the "Cell Zone Conditions" condition) and the upper part of the impeller shaft. The operation of the impeller was modeled assuming a constant rotational speed, without taking into account acceleration or deceleration phases. The calculations were performed for five rotational speed values – the same as in the experiment. In all variants, the effect of gravity was taken into account, and the tank was completely filled with water – without modeling the free surface. A pressure condition of 0 Pa (pressure relative to the environment) was set on the upper surface of the tank. The pressure-velocity coupling was implemented using the SIMPLE algorithm. The SST k-ω model with curvature correction was used to describe turbulent phenomena. The calculation parameters and calculation progress monitors were defined automatically using the "Named Expressions" tool (Table 1). In each case, 1000 iterations were performed, which, according to the data presented in Fig. 8, was considered sufficient to achieve a stable solution.

Table 2

Named expressions used in the numerical model

No.	Name	Expression
1	D	0.195 m
2	I	Backflow Turbulent Intensity (20%)
3	L	Backflow Turbulent Lenght Scale (0.07*D)
4	density	998.2 kg/m^3
5	viscosity	0.001003 kg/(m s)

6	omega	50.26 rad/s
7	n	omega/(2*PI)
8	mixing_power	omega*report_moment
9	power_number	mixing_power/((n^3)*(D^5)*AreaAve(Density,['pressure_outlet']))

Source: own elaboration based on data from ANSYS Fluent.

Figure 10 shows the velocity distribution in a cross-section coinciding with the plane of symmetry of the impeller disk, for the highest rotational speed analyzed. The correct operation of the MRF model and the absence of numerical artifacts at the interface between the moving and stationary zones are visible. The visualization also shows streamlines that illustrate the vortex structures formed in the liquid volume. The arrangement of these structures is characteristic of impellers equipped with a Rushton impeller. The calculated value of the torque for the highest rotational speed was 0.058 N·m, while the value recorded in the experiment was 0.015 N·m.

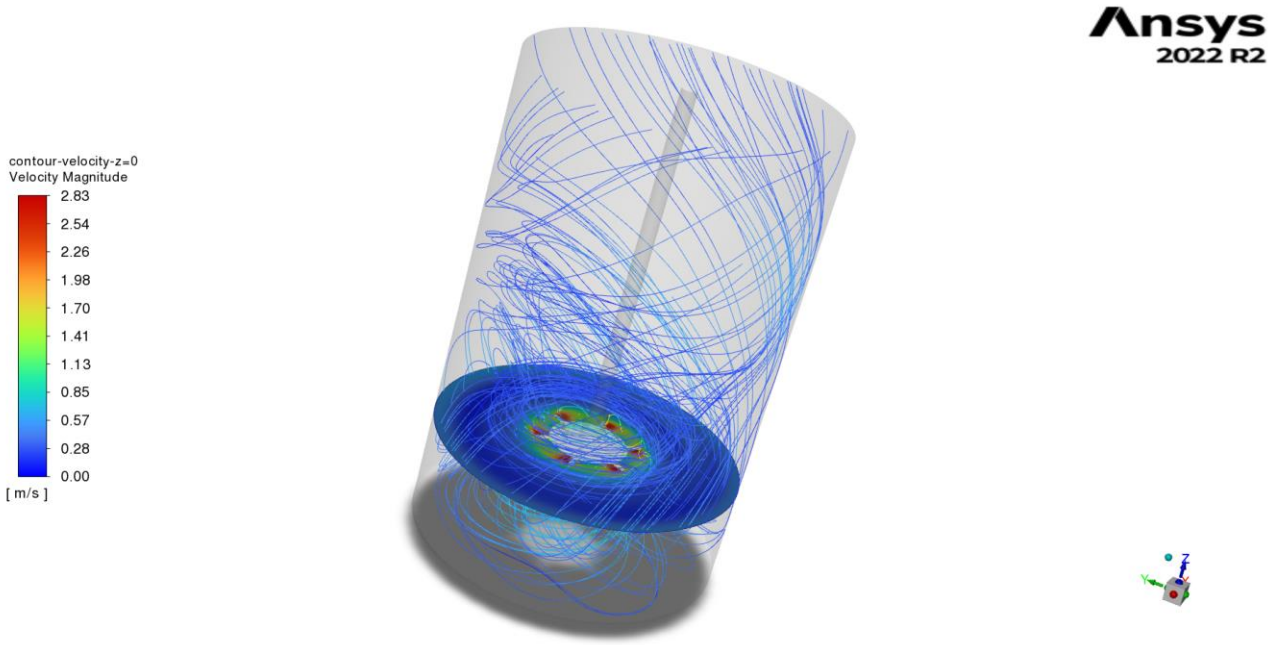

Fig. 10. Velocity distribution at the center of the impeller diskfor the MRF model, 480 rpm, and 1000 iterations

MRF+VoF numerical simulations

The next stage of simulation testing involved performing calculations using the Volume of Fluid (VOF) model, in which air was assumed to be the first phase and water the second phase. The "Implicit Body Force" option was activated in the model and the effect of surface tension forces was taken into account, assuming a value of 0.0072 N/m. The time step was selected to correspond to a 2° rotation of the impeller (the recommended range is 1–5°), which allowed for a more accurate representation of the flow dynamics. The number of time steps was set at 900, which corresponds to five full rotations of the stirrer. The new model variables are listed in Table 3. The calculations were

performed for the highest rotational speed, as the aim of the simulation was to determine a modeling method that would allow higher torques to be obtained, rather than to develop a complete characteristic of the impeller's operation. The use of the VOF model resulted in an increase in the relative calculation time to 1.48. The velocity distribution and streamlines are shown in Figure 11. The calculated value of the torque was 0.063 N·m (compared to the stationary MRF model, the torque increased by less than 10%).

Table 3

Additional named expressions used in the VoF model

No.	Name	Expression
1	angle (2°)	2*0.01745
2	time_step	angle/omega
3	T_rot	2*PI/omega
4	N_iter (5 revolutions)	5*T_rot/time_step

Source: own elaboration based on data from ANSYS Fluent.

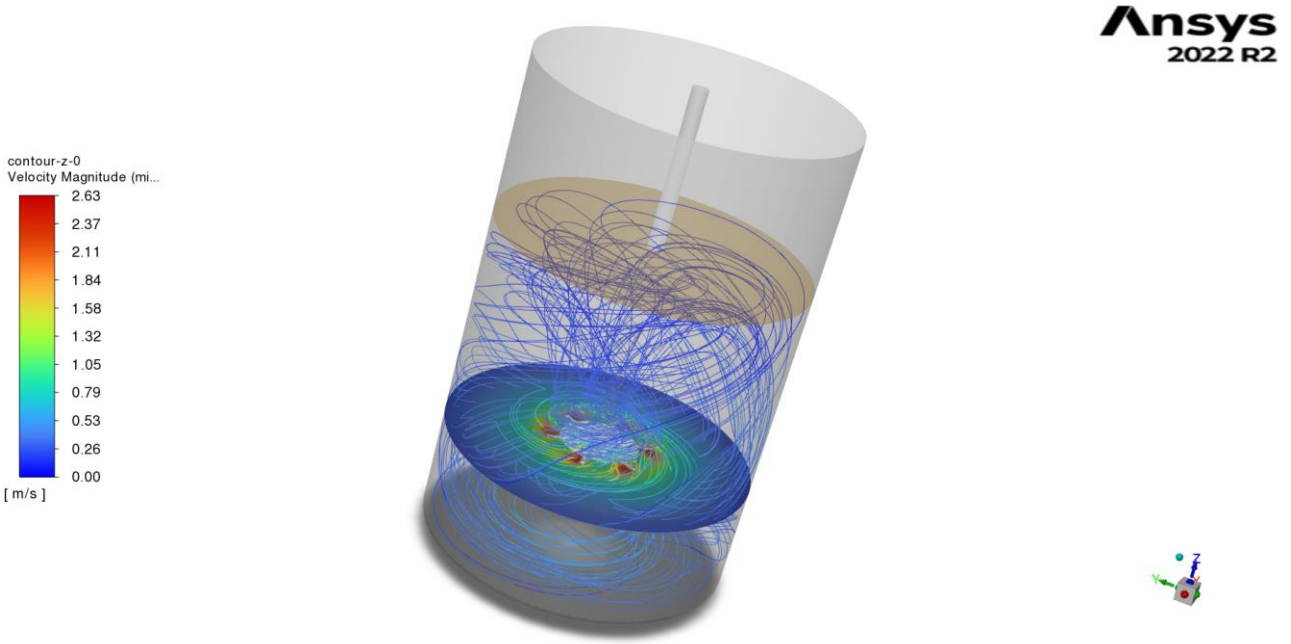

Fig. 11. Velocity distribution at the center of the impeller disk for the MRF+VoF model, 480 rpm, and 1000 iterations

Numerical simulations SM+VoF

In the next part of the simulation studies, an SM model connected to VoF was created. It was decided to analyze this variant as well in order to identify potential causes of discrepancies between the simulation results and the experimental results. The SM model configuration was almost identical to that described in the previous section. The main difference concerned the way the interface was

defined (Fig. 12) – in this case, it was inconsistent. The "Share" tool in the SpaceClaim module was not used, which resulted in the creation of two independent mesh zones with separate sets of nodes.

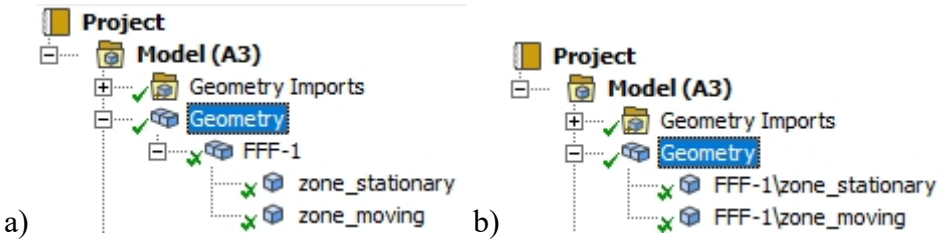

Fig. 12. View of the geometry tree in the Mesh module: a) MRF variant, b) SM variant

The second difference concerned the method of defining the moving zone – instead of the "Frame Motion" option, "Mesh Motion" was enabled. All other settings remained unchanged. Figure 13 shows selected frames from the simulation recording, which show the change in the position of the impeller over time (as indicated by the position of the blades).

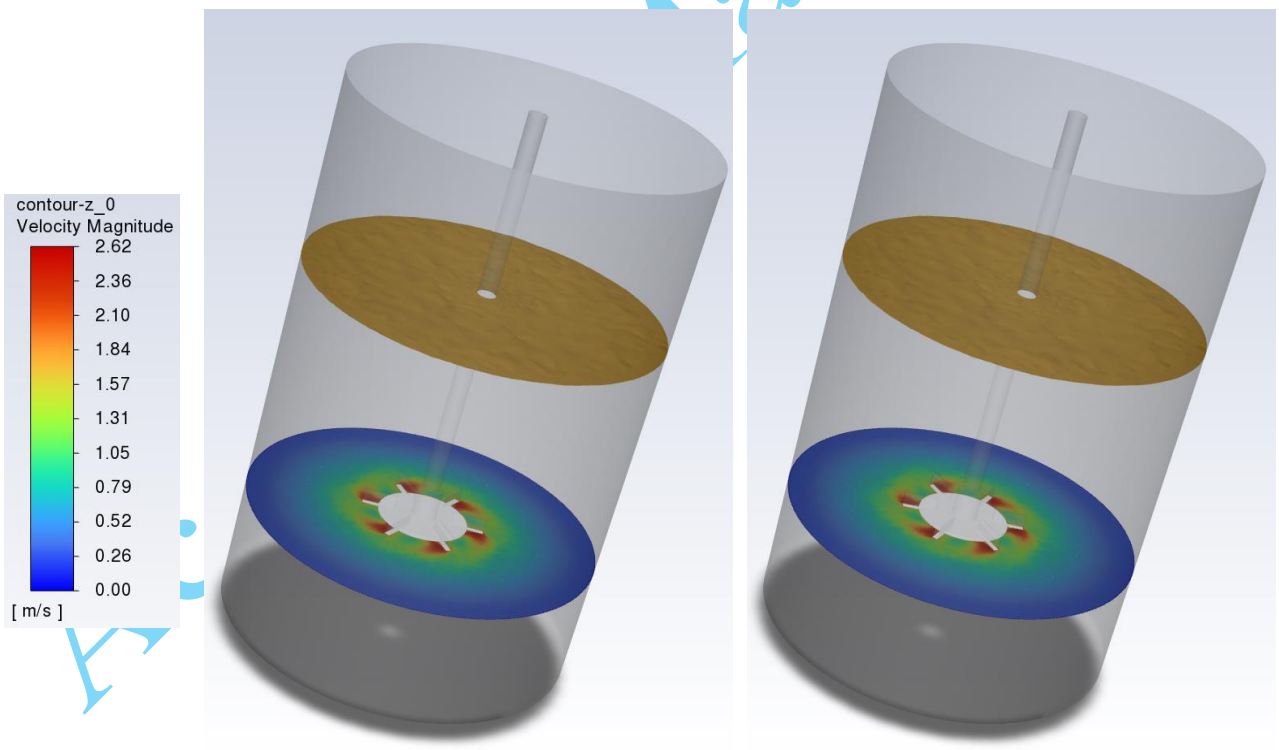

a) b)

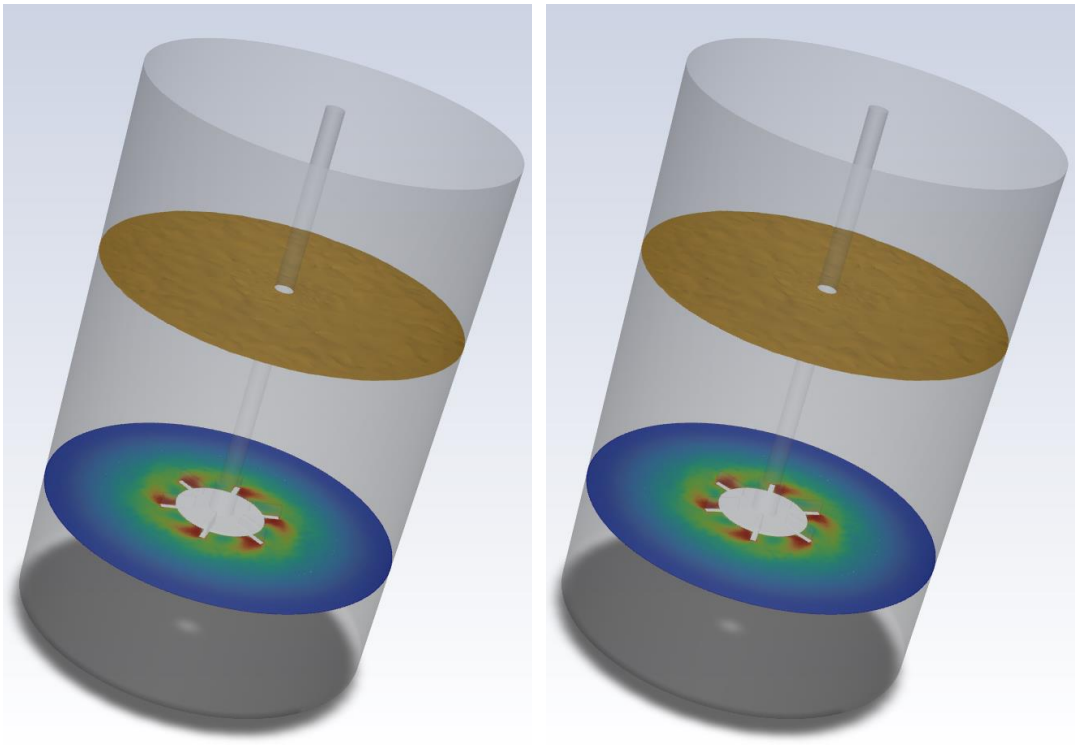

c) d)

Fig. 13. Visualization of the impeller movement: a) iteration 528, b) iteration 532, c) iteration 536, d) iteration 540

It is worth noting that in simulation variants using the Volume of Fluid (VOF) model, no characteristic funnel was observed on the liquid surface – a phenomenon commonly occurring in experimental conditions. Instead, the free surface remained almost completely flat. The likely reason for this was the configuration of the moving zone – its size and position did not fully cover the area immediately within and below the liquid surface. As a result, the mixing in the upper part of the tank may have been insufficiently represented, which limited the possibility of generating a realistic depression of the liquid surface. Due to the priority of experimental verification of the numerical simulation results, a detailed analysis of the funnel formation and adjustment of the geometry of the moving zone were postponed to a later stage of research.

Results and discussion

Figure 14 presents the summary results of numerical and experimental studies. As mentioned earlier, simulations across the entire speed range were performed only for the stationary MRF model and a tank completely filled with liquid. The calculations were performed using the variant analysis available in ANSYS Fluent. For the highest rotational speed, additional MRF simulations were performed for two more densely meshed computational grids in order to assess the impact of grid

density on the determined torque value and to verify the stability of the numerical solution. The torque values obtained for meshes 1 and 2 were practically identical (0.0583 and 0.0584 N·m, respectively), while for mesh 3 they were slightly lower (0.0565 N·m). The results confirm the good repeatability of the calculations and the stability of the solution, while also indicating a slight influence of the mesh density on the obtained torque value.

The numerical characteristics are qualitatively consistent with expectations – the value of the torque increases with increasing rotational speed. This is due to the appearance of higher shear velocities in the liquid and, consequently, higher tangential stresses, which increase the resistance to motion and lead to an increase in torque. The quantitative comparison is less favorable: across the entire analyzed range of torque values, the experimentally determined values are lower than the numerically predicted values. Across the analyzed rotational speed range, the ratio of numerically predicted to experimentally measured torque values varies between individual operating points and amounts on average to approximately 3.42. This number is referred to as the correction factor in further discussions. After dividing the result obtained for MRF (mesh1) by the correction factor, the characteristics overlap, which indicates qualitative consistency of the characteristics and some approximately constant factor causing discrepancies. The use of the VoF model, both in the stationary MRF variant and in the non-stationary SM, did not result in significant quantitative changes. The torque value increased only slightly, reaching 0.0634 and 0.059 N·m, respectively.

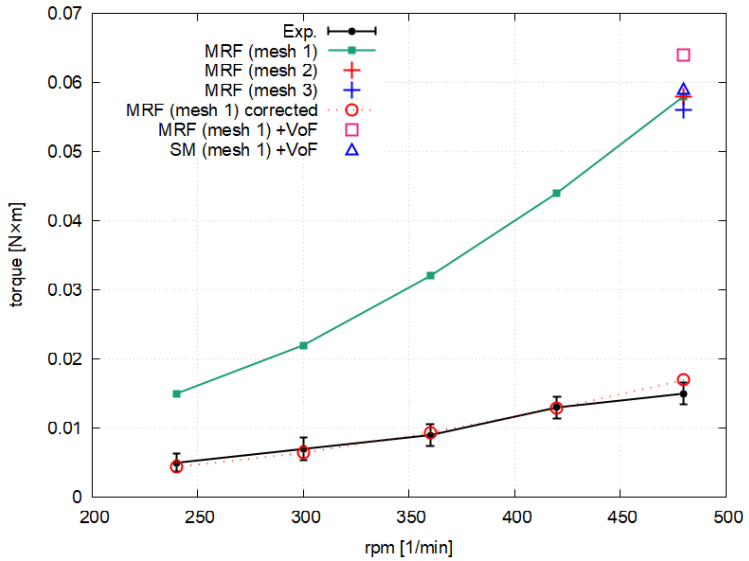

Fig. 14. Torque values as a function of impeller rotational speed

The higher torque values obtained in numerical simulations compared to experimental results

may be related to the absence of a characteristic central funnel in VoF simulations, which in tanks without partitions is a key indicator of the intensity of global momentum transport (HARTMANN et al. 2004, TALAGA, DUDA 2020, PŁUSA et al. 2021, DESHPANDE et al. 2018, PRAKASH et al. 2018). It should be emphasized that the aim of the present study was not to identify optimal operating conditions of an unbaffled Rushton turbine impeller, but to assess the ability of different numerical approaches (MRF and SM, with and without VoF) to predict the impeller torque under experimentally reproducible conditions. For this reason, the rotational speed range was selected to ensure stable and repeatable experimental measurements, even though global flow phenomena such as funnel formation and predominantly circular circulation were observed within the investigated operating range. The lack of a correctly shaped vortex funnel in MRF+VoF and SM+VoF simulations based on RANS models with k-ω SST turbulence indicates the limited ability of these models to reproduce the unsteady global vorticity motion of the fluid, leading to quantitative discrepancies in the determination of torque. Similar limitations of RANS-based approaches in vessels without partitions were pointed out by TAMBURINI et al. (2018) and ZAMIRI (2017). These authors emphasize that in modeling flows in mechanical mixers without partitions, a significant improvement in agreement with experimental results is only achieved when using a non-stationary approach and more advanced, multiscale turbulence models, such as LES (DERKSEN 2001, DELAFOSSE et al. 2009).

The research presented in this article confirms the difficulties encountered in modeling mechanical mixers with non-partitioned tanks using turbulence models from the RANS group. The developed simulation models are useful for analyzing qualitative trends and relative comparisons, but their ability to quantitatively predict torque in their current form remains limited. At this stage of research, it is not known whether the correction factor is constant or depends on the specific geometry of the impeller, and if so, how strongly. In further work, it is reasonable to improve the quality and reliability of experimental data, including considering the construction of a dedicated measurement station, as well as to develop numerical modeling towards Sliding Mesh unsteady simulations in combination with LES models. This approach should enable better representation of vortex structures, free surface deformation of the liquid, and central funnel formation, and consequently improve the quantitative agreement of simulation results with experimental data.

Conclusions

The research conducted allowed us to formulate the following observations and conclusions:

- The developed numerical models of a cylindrical mechanical mixer without partitions with a Rushton impeller enable correct mapping of the qualitative characteristics of the flow,

including the torque characteristics as a function of the impeller speed M(rpm). Good agreement between numerical and experimental trends was obtained, while quantitative agreement remains limited.

- Analysis of the impact of computational mesh density, conducted for the highest rotational speed, demonstrated good stability and repeatability of the numerical solution, as well as its low sensitivity to mesh density.
- The results obtained using the MRF+VoF and SM+VoF approaches did not lead to a significant improvement in the consistency of the results, which indicates that the observed discrepancies are primarily due to the influence of other factors.
- Across the entire analyzed speed range, the torque values obtained in numerical simulations are higher than those determined experimentally. The observed differences may result from several coexisting factors, in particular:
  - measurement uncertainties resulting from the characteristics of the IKA EUROSTAR 60 control drive used, in particular operation in the lower torque measurement range, which could lead to increased relative errors;
  - limitations of the adopted numerical approach based on RANS models, which have a limited ability to reproduce unsteady, global vortex motion of liquids in tanks without partitions;
  - lack of correct mapping of free surface deformation of liquids, including the characteristic vortex funnel, which is an important indicator of momentum transport intensity in such systems.

Acknowledgements:

The authors would like to express their sincere gratitude to Dr. hab. Eng. Fabian Dajnowiec, Head of the Department of Engineering, Process Equipment and Food Biotechnology at the University of Warmia and Mazury in Olsztyn, for granting permission to use the experimental equipment available at his department and for enabling the research presented in this study. The authors also thank Dr. Eng. Józef Warechowski for his valuable assistance in performing the experimental measurements.

References

ALAM Z., KUMAR C., AVATAR K., MAZUMDAR D. 2022. *Modeling of Fluid Flow and Bulk Liquid Mixing Phenomena in a Mechanically Agitated Ladle.* Metallurgical and Materials Transactions B, 53(1): 304-319. https://doi.org/10.1007/s11663-021-02367-4

Ansys Fluent Theory Guide. 2022. Release 2022 R1, January 2022.

DELAFOSSE A., MORCHAIN J., GUIRAUD P., LINÉ A. 2009. *Trailing vortices generated by a Rushton turbine: Assessment of URANS and large eddy simulations.* Chemical Engineering Research and Design, 87(4): 401-411. https://doi.org/10.1016/j.cherd.2008.12.018

DERKSEN J.J. 2001. *Assessment of large eddy simulations for agitated flows.* Chemical Engineering Research and Design, 79(7): 824-830. https://doi.org/10.1205/02638760152721334

DESHPANDE S.S., KAR K.K., WALKER J., PRESSLER J., SU W. 2017. *An experimental and computational investigation of vortex formation in an unbaffled stirred tank.* Chemical Engineering Science, 168: 495-506. https://doi.org/10.1016/j.ces.2017.04.002

HARTMANN H., DERKSEN J.J., VAN DEN AKKER H.E.A. 2004. *Macroinstability uncovered in a Rushton turbine stirred tank.* AIChE Journal, 50(6): 1305-1315. https://doi.org/10.1002/aic.10211

KOYRO P.T., DE MOURA H.L., DE LIMA AMARAL R., DE LIMA E FREITAS L.F., BARBUTTI A.D., NUNHEZ J.R., DE CASTILHO G.J. 2022. *Comparison of PIV measurements and OpenFOAM simulations of a stirred tank: study of the azimuthal position effect*. Journal of the Brazilian Society of Mechanical Sciences and Engineering, 44: 421. https://doi.org/10.1007/s40430-022-03713-6

KYSELA B., KONFRŠT J., FOŘT I., CHÁRA Z. 2014. *CFD Simulation of the Discharge Flow from Standard Rushton Impeller*. International Journal of Chemical Engineering, 706149: 1-7. http://dx.doi.org/10.1155/2014/706149

PATIL H., PATEL A., PANT H., ANANTHULA V. 2018. *CFD simulation model for mixing tank using multiple reference frame (MRF) impeller rotation*. ISH Journal of Hydraulic Engineering, 27. https://doi.org/10.1080/09715010.2018.1535921

PHUMNOK E., SAETIAO P., BUMPHENKIATTIKUL P., RATTANAWILAI S., KHONGPROM P. 2024. *CFD simulation of silica dispersion/natural rubber latex mixing for high silica content rubber composite production*. RSC Advances, 14(18): 1-12. http://dx.doi.org/10.1039/D4RA01348D

PŁUSA T., TALAGA K., DUDA A., DUDA P. 2021. *Modeling mixing dynamics in uncovered baffled and unbaffled stirred tanks.* Chemical Engineering Research and Design, 169: 287-301. https://doi.org/10.1016/j.cherd.2021.03.020

PRAKASH B., BHATELIA T., WADNERKAR D., SHAH M.T., PAREEK V.K., UTIKAR R.P. 2018. *Vortex shape and gas–liquid hydrodynamics in unbaffled stirred tank.* The Canadian Journal of Chemical Engineering, 97(6): 1913-1920. https://doi.org/10.1002/cjce.23433

SOBIESKI W. 2025. *Challenges in Simulating Pollutant Behavior in Watercourses with Diverse Ecological and Structural Features*. Journal of Applied Fluid Mechanics, 18(8): 1964-1979. https://doi.org/10.47176/jafm.18.8.3269

STREK F. 1971. *Mieszanie i Mieszalniki (Mixing and Mixers)*. Wydawnictwo Naukowo-Techniczne, Warszawa.

TALAGA K., DUDA P. 2020. *Identification of the liquid turbulent flow based on experimental methods.* International Journal of Applied Fluid Mechanics, 13(6): 1903-1914. https://doi.org/10.47176/jafm.13.06.32791

TAMBURINI A., GAGLIANO G., MICALE G., BRUCATO A., SCARGIALI F., CIOFALO M. 2018. *Direct numerical simulations of creeping to early turbulent flow in unbaffled and baffled stirred tanks.* Chemical Engineering Science, 192: 161–175. https://doi.org/10.1016/j.ces.2018.07.023

TILL Z., MOLNÁR B., EGEDY A., VARGA T. 2019. *CFD Based Qualification of Mixing Efficiency of Stirred Vessels*. Periodica Polytechnica Chemical Engineering, 63(1): 226-238. https://doi.org/10.3311/PPch.12245

ZAMIRI A. 2017. *Ability of URANS approach in prediction of unsteady turbulent flows in an unbaffled stirred tank.* International Journal of Mechanical Sciences, 133: 178-187. https://doi.org/10.1016/j.ijmecsci.2017.08.008